

## Magnetic and crystal structures of the polymorphic Pr<sub>5</sub>Si<sub>2</sub>Ge<sub>2</sub> compound

Y. C. Wang,<sup>1</sup> H. F. Yang,<sup>1</sup> Q. Huang,<sup>2</sup> L. B. Duan,<sup>1</sup> J. W. Lynn,<sup>2</sup> and G. H. Rao<sup>1,\*</sup>

<sup>1</sup>Beijing National Laboratory for Condensed Matter Physics, Institute of Physics, Chinese Academy of Sciences, Beijing 100080, People's Republic of China

<sup>2</sup>NIST Center for Neutron Research, National Institute of Standards and Technology, Gaithersburg, Maryland 20899-8562, USA

(Received 25 April 2007; revised manuscript received 18 June 2007; published 21 August 2007)

Crystallographic and magnetic structures of the polymorphisms of Pr<sub>5</sub>Si<sub>2</sub>Ge<sub>2</sub> compound: the tetragonal *t*-Pr<sub>5</sub>Si<sub>2</sub>Ge<sub>2</sub> and the monoclinic *m*-Pr<sub>5</sub>Si<sub>2</sub>Ge<sub>2</sub>, are investigated by neutron powder diffraction at different temperatures. The *t*-Pr<sub>5</sub>Si<sub>2</sub>Ge<sub>2</sub> crystallizes in the Zr<sub>5</sub>Si<sub>4</sub>-type structure with the space group *P*4<sub>1</sub>2<sub>1</sub>2 down to 4 K. Long-range magnetic ordering takes place at  $T_C=52$  K, and the magnetic structure can be modeled with the magnetic space group *P*4<sub>1</sub>2<sub>1</sub>'2'. The net magnetic moment occurs exclusively along the *c* direction. The lattice parameters change continuously around  $T_C$  with a small negative magnetovolume effect, indicating a second-order phase transition. The *m*-Pr<sub>5</sub>Si<sub>2</sub>Ge<sub>2</sub> crystallizes in the Gd<sub>5</sub>Si<sub>2</sub>Ge<sub>2</sub>-type structure with the space group *P*112<sub>1</sub>/*a* down to 4 K. Long-range magnetic ordering occurs at  $T_C=40$  K and the magnetic structure can be modeled with the magnetic space group *P*112<sub>1</sub>'/*a*'. The net magnetic moment lies on the *ab* plane, with the main component along the *a* axis. No other magnetic transition is observed below  $T_C$  for both the compounds, and the largest shrinking of lattice parameter upon cooling through  $T_C$  occurs along the direction with the largest net magnetic moment component. The relatively stable existence at room temperature of the polymorphic Pr<sub>5</sub>Si<sub>2</sub>Ge<sub>2</sub> is readily understood based on the correlation between the crystal structures of *t*-Pr<sub>5</sub>Si<sub>2</sub>Ge<sub>2</sub> and *m*-Pr<sub>5</sub>Si<sub>2</sub>Ge<sub>2</sub>. In the scenario of the Ruderman-Kittel-Kasuya-Yosida interaction model, the complex noncollinear magnetic structures of the compounds can be attributed to a competition of different Pr-Pr exchange interactions due to the different chemical environments around Pr atoms on different sites and to the broad range of the Pr-Pr distances.

DOI: 10.1103/PhysRevB.76.064425

PACS number(s): 75.25.+z, 75.30.Kz, 75.30.Sg

### I. INTRODUCTION

The discovery of giant magnetocaloric effect (MCE) in Gd<sub>5</sub>Si<sub>2</sub>Ge<sub>2</sub> by Pecharsky and Gschneidner<sup>1</sup> has renewed the interest in recent years in the family of intermetallic compounds  $R_5(\text{Si}_x\text{Ge}_{1-x})_4$  ( $R$ =rare earth metal), which were known and studied 40 years ago.<sup>2</sup> The incidence of the MCE in Gd<sub>5</sub>Si<sub>2</sub>Ge<sub>2</sub> is closely related to a simultaneous occurrence of the first-order magnetic and martensiticlike structural phase transitions.<sup>3,4</sup> The strong coupling of magnetic and crystallographic sublattices is also responsible for the strong magnetoelastic effect<sup>3,5</sup> and the giant magnetoresistance<sup>6</sup> in Gd<sub>5</sub>(Si<sub>*x*</sub>Ge<sub>1-*x*</sub>)<sub>4</sub>. Knowledge of magnetic and crystallographic structures of these compounds is obviously indispensable for understanding the microscopic physical mechanisms controlling the observed intriguing behavior. The magnetic structure of Gd<sub>5</sub>Ge<sub>4</sub> was recently elucidated from x-ray resonant magnetic scattering data,<sup>7</sup> yet the determination of the magnetic structures of Gd<sub>5</sub>(Si<sub>*x*</sub>Ge<sub>1-*x*</sub>)<sub>4</sub> by neutron diffraction remains a challenge due to the huge neutron absorption cross section of the majority Gd isotope. Therefore, the magnetic structures of many binary and pseudobinary compounds  $R_5(\text{Si}_x\text{Ge}_{1-x})_4$  other than  $R=\text{Gd}$  have been extensively visited or revisited recently.<sup>8-15</sup> In the study of Tb<sub>5</sub>(Si<sub>1-*x*</sub>Ge<sub>*x*</sub>)<sub>4</sub> system, Ritter *et al.* found that Tb<sub>5</sub>Si<sub>2</sub>Ge<sub>2</sub> crystallized in monoclinic paramagnetic Gd<sub>5</sub>Si<sub>2</sub>Ge<sub>2</sub>-type structure (space *P*112<sub>1</sub>/*a*) at room temperature and in the orthorhombic ferromagnetic Gd<sub>5</sub>Si<sub>4</sub>-type structure (space group *Pnma*) at low temperature.<sup>10</sup> In contrast to the Gd<sub>5</sub>Si<sub>2</sub>Ge<sub>2</sub>, however, the paramagnetic monoclinic Tb<sub>5</sub>Si<sub>2</sub>Ge<sub>2</sub> first transformed to a monoclinic ferromagnetic structure ( $T_C=110$  K) before the

further transition to the orthorhombic ferromagnetic Gd<sub>5</sub>Si<sub>4</sub>-type structure ( $T_f=100$  K) on cooling, indicating that the structural and magnetic transitions are not fully coupled in Tb<sub>5</sub>Si<sub>2</sub>Ge<sub>2</sub>.<sup>11</sup> The monoclinic ferromagnetic structure was also stable down to 4 K in Nd<sub>5</sub>Si<sub>1.45</sub>Ge<sub>2.55</sub> and Pr<sub>5</sub>Si<sub>1.5</sub>Ge<sub>2.5</sub> (Ref. 12) and in Er<sub>5</sub>(Si<sub>*x*</sub>Ge<sub>1-*x*</sub>)<sub>4</sub>.<sup>15</sup> In particular, Er<sub>5</sub>Si<sub>4</sub> crystallized in the Gd<sub>5</sub>Si<sub>4</sub>-type structure at room temperature and underwent a structural transition to the lower symmetry monoclinic structure (Gd<sub>5</sub>Si<sub>2</sub>Ge<sub>2</sub>-type, *P*112<sub>1</sub>/*a*) upon cooling in the temperature range between 160 and 220 K, whereas magnetic ordering developed below the structural transition temperature ( $T_C=30$  K) and the crystallographic structure retained the monoclinic symmetry.<sup>15,16</sup>

Another intriguing feature of Gd<sub>5</sub>(Si<sub>*x*</sub>Ge<sub>1-*x*</sub>)<sub>4</sub> is the polymorphic behavior in paramagnetic state around  $x=0.5$ . Monoclinic Gd<sub>5</sub>Si<sub>2</sub>Ge<sub>2</sub> underwent an elastic transformation to high temperature Gd<sub>5</sub>Si<sub>4</sub>-type structure in the temperature range of 573–593 K upon heating, which was reversible during heating and slow cooling but irreversible during rapid cooling.<sup>17</sup> However, the transformation of monoclinic Gd<sub>5</sub>Si<sub>2.09</sub>Ge<sub>1.91</sub> to high temperature Gd<sub>5</sub>Si<sub>4</sub>-type structure became sluggish, incomplete and irreversible between room temperature and 730 K.<sup>18</sup> It is noteworthy that the lower symmetry monoclinic Gd<sub>5</sub>Si<sub>2.09</sub>Ge<sub>1.91</sub> was prepared by heat-treating the as-arc melted counterpart, which crystallized in the higher symmetry orthorhombic Gd<sub>5</sub>Si<sub>4</sub>-type structure, at 1570 K for 7 h followed by a fairly rapid cooling to room temperature and the resulting alloy contained ~14 vol % of the orthorhombic phase. The magnetization curves of the as-arc-melted and heat-treated samples at 10 kOe (*M-T* curves) showed little difference, except that the Curie temperature of

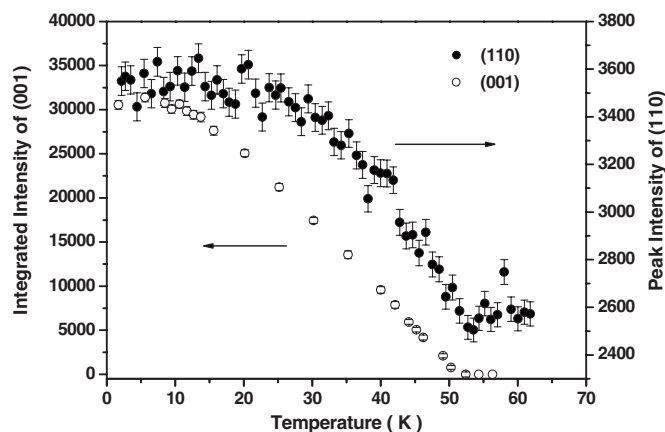


FIG. 1. Temperature dependence of the integrated intensity of (001) peak and the peak intensity of (110) reflection of  $t\text{-Pr}_5\text{Si}_2\text{Ge}_2$  on warming, measured by high-flux BT-7 spectrometer at NIST-NCNR.

the monoclinic phase was about 5 K lower than that of the orthorhombic phase. The monoclinic phase exhibited the first-order magnetic-martensiticlike structural transitions around  $T_C$  ( $\sim 295$  K), whereas the orthorhombic phase showed exclusively the normal second-order paramagnetic-ferromagnetic transition at  $T_C$  ( $\sim 300$  K).<sup>18</sup>

Polymorphism was also observed in  $\text{Pr}_5\text{Si}_2\text{Ge}_2$ , but the features of the structural transition and the structure dependence of physical properties were distinguished from those of  $\text{Gd}_5\text{Si}_2\text{Ge}_2$ .<sup>19</sup> In the study of  $\text{Pr}_5(\text{Si}_x\text{Ge}_{1-x})_4$  system, Yang *et al.* found that the as-arc-melted  $\text{Pr}_5\text{Si}_2\text{Ge}_2$  crystallized in the monoclinic  $\text{Gd}_5\text{Si}_2\text{Ge}_2$ -type structure ( $m\text{-Pr}_5\text{Si}_2\text{Ge}_2$ ,  $P112_1/a$ ) at room temperature with a minor tetragonal phase ( $\sim 3$  wt %) and the high purity single-phase tetragonal  $\text{Pr}_5\text{Si}_2\text{Ge}_2$  ( $t\text{-Pr}_5\text{Si}_2\text{Ge}_2$ ) could be fabricated by annealing the as-arc-melted  $m\text{-Pr}_5\text{Si}_2\text{Ge}_2$  at 1273 K followed by a water quench. The  $t\text{-Pr}_5\text{Si}_2\text{Ge}_2$  crystallized in the  $\text{Zr}_5\text{Si}_4$ -type structure (space group  $P4_12_12$ ), which is taken by many light rare earth silicides ( $R_5\text{Si}_4$ ). X-ray powder diffraction (XRD) showed that annealing the samples at 873 K for two months did not result in noticeable change of the XRD patterns for both the  $m\text{-Pr}_5\text{Si}_2\text{Ge}_2$  and the  $t\text{-Pr}_5\text{Si}_2\text{Ge}_2$ , indicating their relatively stable character at room temperature. The magnetization and electronic transport properties of these two compounds exhibited similar behavior, but their magnetic ordering temperatures differed by more than 10 K. At 5 K and 50 kOe, both compounds manifested a magnetic moment per Pr atom much lower than the saturation value of a free  $\text{Pr}^{3+}$  ion ( $3.5\mu_B$ ), possibly implying complex noncollinear magnetic structures at low temperature, although the effects due to the presence of crystalline electric field (CEF) and large magnetocrystalline anisotropy cannot be ruled out. In the present work, the crystallographic and magnetic structures of the polymorphic  $\text{Pr}_5\text{Si}_2\text{Ge}_2$  ( $m$ - and  $t\text{-Pr}_5\text{Si}_2\text{Ge}_2$ ) in the temperature range between 4 and 300 K are studied by means of neutron powder diffraction. After a brief description of experiments in Sec. II, the refinement results of the crystal and magnetic structures at different temperatures are presented in Sec. III. A discussion on the magnetic structures and the

correlation between the crystal structures of the  $m$ - and  $t\text{-Pr}_5\text{Si}_2\text{Ge}_2$  is given in Sec. IV, and a summary of the work in Sec. V.

## II. EXPERIMENT

Details of the preparation of alloy samples have been described in Ref. 19. Polycrystalline  $\text{Pr}_5\text{Si}_2\text{Ge}_2$  alloy was prepared by arc melting the corresponding mixtures of pure metal components (with purity better than 99.9% for Pr and 99.9999% for Si and Ge) in a water-cooled copper hearth under an argon atmosphere. The alloy was arc melted 4–5 times, with the alloy button being turned over after each melting to improve the homogeneity of the alloy. Part of the as-arc-melted alloy was sealed in an evacuated quartz tube and annealed at 1273 K for one week, followed by a water quench. The chemical compositions of both the as-arc-melted and the heat-treated samples were determined to be in good agreement with the nominal compositions by means of an inductively coupled plasma atomic emission spectroscopy (TJACo.). XRD (Rigaku D/max 2500,  $\text{Cu K}\alpha$  radiation,  $50\text{ kV} \times 250\text{ mA}$ ) showed that the as-arc-melted sample crystallized in the monoclinic  $\text{Gd}_5\text{Si}_2\text{Ge}_2$ -type structure ( $P112_1/a$ ) and the heat-treated sample in the tetragonal  $\text{Zr}_5\text{Si}_4$ -type structure ( $P4_12_12$ ). The as-arc-melted and the heat-treated samples are referred hereafter as  $m\text{-Pr}_5\text{Si}_2\text{Ge}_2$  and  $t\text{-Pr}_5\text{Si}_2\text{Ge}_2$ , respectively.

Neutron powder diffraction (NPD) experiments in the temperature range between 4 and 300 K were performed at the NIST Center for Neutron Research (NCNR). The magnetic ordering was first examined on the high-flux BT-7 spec-

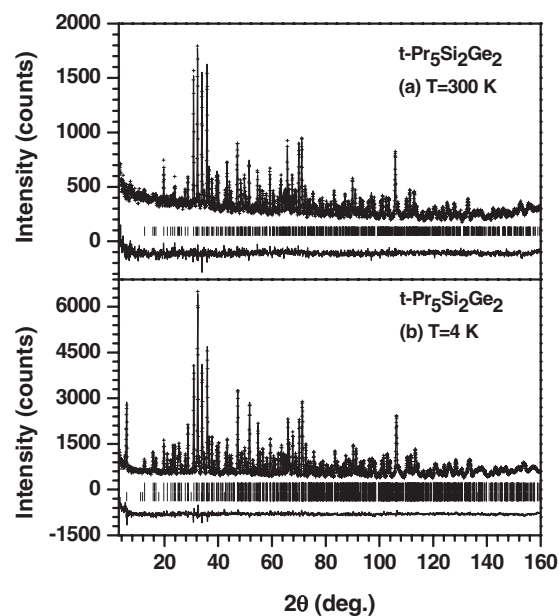


FIG. 2. Experimental (crosses) and calculated (solid line) intensities of  $t\text{-Pr}_5\text{Si}_2\text{Ge}_2$  at (a) 300 K and (b) 4 K. Differences between the experimental and calculated patterns are shown at the bottom of the figure. The vertical bars indicate the expected nuclear reflection positions. The expected magnetic reflection positions are marked by the bars on the lower row in (b).

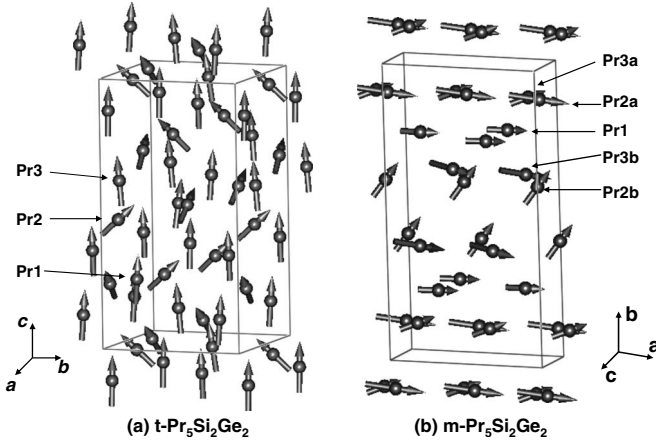


FIG. 3. The magnetic structure of (a)  $t\text{-Pr}_5\text{Si}_2\text{Ge}_2$  and (b)  $m\text{-Pr}_5\text{Si}_2\text{Ge}_2$ . Only the magnetic atoms are shown.

trometer with a neutron wavelength of 2.4649 Å provided by a pyrolytic graphite monochromator and filter. The NPD data for refinements of the crystallographic and magnetic structures were collected on the high-resolution, 32-counter BT-1 diffractometer. Monochromatic neutron beam of wavelength 1.5403(1) Å was used for the  $t\text{-Pr}_5\text{Si}_2\text{Ge}_2$  and a wavelength of 2.0787 Å for the  $m\text{-Pr}_5\text{Si}_2\text{Ge}_2$ . The NPD data were collected in the  $2\theta$  range of  $3^\circ\text{--}168^\circ$  with a step of  $0.05^\circ$ . The program FULLPROF (Ref. 20) was used for the Rietveld refinement of the crystallographic and magnetic structures of the compounds.

### III. RESULTS

#### A. Crystal and magnetic structures of $t\text{-Pr}_5\text{Si}_2\text{Ge}_2$

Neutron powder diffraction at room temperature confirms that the investigated sample is single phase and crystallizes in the tetragonal  $\text{Zr}_5\text{Si}_4$ -type structure. The NPD pattern can be well indexed by the space group  $P4_12_12$ . On cooling the sample, the (001) peak develops around  $2\theta=6^\circ$ , which is forbidden by the space group  $P4_12_12$  and is attributed to a purely magnetic contribution. In the temperature range between 4 and 300 K, no reflection with fractional index is observed, suggesting the same unit cell for the crystallographic and magnetic structures. Figure 1 shows the evolutions of the integrated intensity of the (001) peak and the peak intensity of the (110) reflection on warming, and both indicate that the long-range magnetic ordering disappears around  $T_C=52$  K, in good coincidence with the magnetization measurements ( $T_C=50$  K).<sup>19</sup> No other magnetic transition occurs below  $T_C$ .

High-resolution NPD data were recorded at 13 temperatures: 4, 10, 20, 30, 40, 50, 60, 70, 100, 150, 200, 250, and 300 K. The NPD data of  $T > T_C$  are attributed exclusively to nuclear scattering and can be refined with the space group  $P4_12_12$  as shown in Fig. 2(a) and Table I. Single-crystal XRD work suggested a nonstatistical distribution of Si and Ge in monoclinic  $\text{Gd}_5(\text{Si}_{1-x}\text{Ge}_x)_4$  compounds,<sup>4,17</sup> so we attempted to refine the occupancies of Si and Ge in  $t\text{-Pr}_5\text{Si}_2\text{Ge}_2$ . For the NPD data at 300 K, the derived Si/Ge

TABLE I. Data of crystallographic structure at selected temperatures for  $t\text{-Pr}_5\text{Si}_2\text{Ge}_2$  derived from the fitting to NPD patterns. Space group:  $P4_12_12$ .  $M=0.5\text{Si}+0.5\text{Ge}$ ,  $B$  is the isotropic temperature factor, and  $R_P$  and  $R_{WP}$  are residuals of fitting to the pattern and the weighted pattern, respectively.  $R_B$  and  $R_M$  are Bragg and magnetic  $R$  factors, respectively.  $\chi^2$  is a “goodness of fit” indicator (Ref. 20).

	4 K	40 K	60 K	300 K
$a$ (Å)	7.94849(9)	7.9455(3)	7.9442(2)	7.9667(2)
$c$ (Å)	14.9168(2)	14.9282(6)	14.9395(4)	14.9297(5)
$V$ (Å <sup>3</sup> )	942.42(2)	942.42(6)	942.84(4)	947.56(5)
Pr1 (4a) $x$	0.3126(4)	0.3132(9)	0.3142(6)	0.3141(9)
$B$ (Å <sup>2</sup> )	0.60(3)	0.49(8)	0.60(4)	1.14(6)
Pr2 (8b) $x$	0.3670(3)	0.3664(9)	0.3668(5)	0.3657(6)
$y$	0.0107(3)	0.0109(9)	0.0112(5)	0.0118(7)
$z$	0.4545(1)	0.4540(5)	0.4543(2)	0.4552(3)
$B$ (Å <sup>2</sup> )	0.54(2)	0.55(5)	0.64(3)	0.87(4)
Pr3 (8b) $x$	0.1336(3)	0.1334(7)	0.1336(5)	0.1352(7)
$y$	-0.0145(3)	-0.0138(7)	-0.0145(4)	-0.0136(6)
$z$	0.8742(3)	0.8749(8)	0.8754(5)	0.8747(6)
$B$ (Å <sup>2</sup> )	0.47(2)	0.47(5)	0.51(3)	1.05(4)
$M1$ (8b) $x$	0.1993(3)	0.1991(7)	0.1990(4)	0.2003(5)
$y$	0.1625(3)	0.1617(7)	0.1619(4)	0.1625(5)
$z$	0.6929(1)	0.6924(3)	0.6928(2)	0.6920(2)
$B$ (Å <sup>2</sup> )	0.51(2)	0.51(5)	0.67(3)	0.88(3)
$M2$ (8b) $x$	0.2909(3)	0.2903(8)	0.2911(4)	0.2922(6)
$y$	0.9314(3)	0.9325(8)	0.9312(4)	0.9329(5)
$z$	0.0609(1)	0.0612(3)	0.0608(2)	0.0619(2)
$B$ (Å <sup>2</sup> )	0.54(2)	0.60(5)	0.61(3)	0.98(3)
$R_P(\%)/R_{WP}(\%)$	3.68/4.34	8.49/10.0	4.22/5.18	4.19/5.25
$R_B(\%)/R_M(\%)$	4.24/7.37	7.37/14.1	6.15/ $N$	7.61/ $N$
$\chi^2$	1.36	0.869	0.958	0.904

occupancy ratios are 0.51/0.49 on  $M1$  site with  $B(M1)=0.85$  Å<sup>2</sup>, 0.49/0.51 on  $M2$  site with  $B(M2)=1.02$  Å<sup>2</sup> when the total Si/Ge ratio was fixed to 1, and 0.46/0.54 on  $M1$  site with  $B(M1)=0.92$  Å<sup>2</sup>, 0.43/0.57 on  $M2$  site with  $B(M2)=1.12$  Å<sup>2</sup> if the total Si/Ge ratio was not fixed. In comparison with the data in Table I, the thermal parameter  $B$  increases with the Ge occupancy on each site, which could be due to possible correlation between  $B$  and occupancy in the refinement. For the  $m\text{-Pr}_5\text{Si}_2\text{Ge}_2$ , our previous refinement of powder XRD data at 300 K did not detect any preferential occupation of the Ge and Si atoms,<sup>21</sup> and the refinement of the present NPD data at 300 K shows similar correlation between  $B$  and Ge occupancy as that for the  $t\text{-Pr}_5\text{Si}_2\text{Ge}_2$ . Moreover, in contrast to the single-crystal XRD work on  $\text{Gd}_5\text{Si}_2\text{Ge}_2$ , the refinement of NPD data shows that in  $m\text{-Pr}_5\text{Si}_2\text{Ge}_2$  the occupancy of Ge atoms is larger than 0.5 on the  $M1$  and  $M3a$  sites and smaller than 0.5 on the  $M2$  and

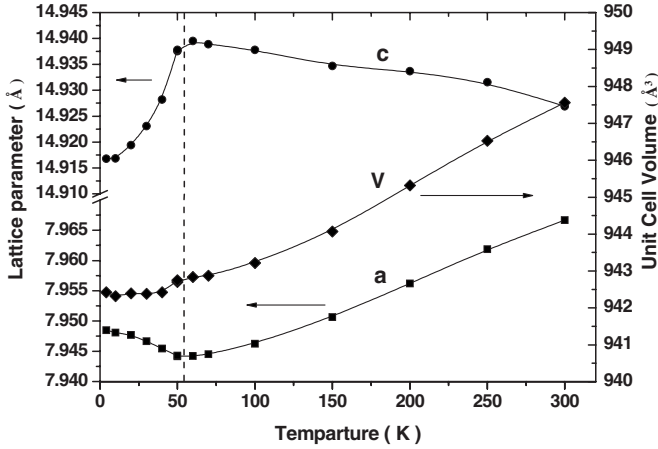


FIG. 4. Temperature dependence of the lattice parameters of  $t$ - $\text{Pr}_5\text{Si}_2\text{Ge}_2$ . The vertical dashed line indicates the position of  $T_C$ .

$M3b$  sites, while the single-crystal XRD work suggested Ge atoms should preferentially occupy both the  $M3a$  and  $M3b$  sites.<sup>4,17</sup> Therefore, we are unable to reach a conclusive result regarding the nonstatistical distribution of the Si and Ge atoms in  $\text{Pr}_5\text{Si}_2\text{Ge}_2$  based on the powder diffraction data and will assume a random distribution of the atoms on each site as in many reported powder diffraction works on  $R_5(\text{Si}_{1-x}\text{Ge}_x)_4$  compounds<sup>10,12,15</sup>

The NPD data of  $T < T_C$  comprise scattering contributions of both the nuclear and magnetic lattices. Since the  $t$ - $\text{Pr}_5\text{Si}_2\text{Ge}_2$  exhibited appreciable magnetization at 5 K and 50 kOe, possible magnetic structure models should have large ferromagnetic components. A magnetic space group compatible with nonzero total magnetic component should be a ferromagnetic one.<sup>22</sup> Other magnetic space groups result in a null resultant spin vector of the atoms on each equivalent site, i.e., an antiferromagnetic (AFM) arrangement. There are 275 ferromagnetic space groups among 1651 Shubnikov groups (see Table III in Ref. 22). Thus, if the magnetization curve of a compound exhibits ferromagnetic (FM) or ferrimagnetic (FIM) behavior without a sign of AFM-FM or AFM-FIM metamagnetic transition, the number of possible

TABLE II. Magnetic moment components of Pr atoms in  $t$ - $\text{Pr}_5\text{Si}_2\text{Ge}_2$  at selected temperatures derived from the fitting to NPD data. The atomic positions refer to Table I. Magnetic space group:  $P4_12_1'2'$ .

	$\mu_x$ ( $\mu_B$ )	$\mu_y$ ( $\mu_B$ )	$\mu_z$ ( $\mu_B$ )	$\mu$ ( $\mu_B$ )
$T=4$ K				
Pr1	-0.29(3)	0.29(3)	2.75(4)	2.78(4)
Pr2	0.18(5)	-1.86(3)	1.69(3)	2.52(3)
Pr3	0.23(5)	0.01(3)	2.81(3)	2.82(3)
$T=40$ K				
Pr1	-0.20(12)	0.20(12)	2.46(12)	2.47(12)
Pr2	0.19(16)	-1.09(10)	1.10(8)	1.56(10)
Pr3	-0.04(20)	-0.03(10)	2.24(7)	2.24(7)

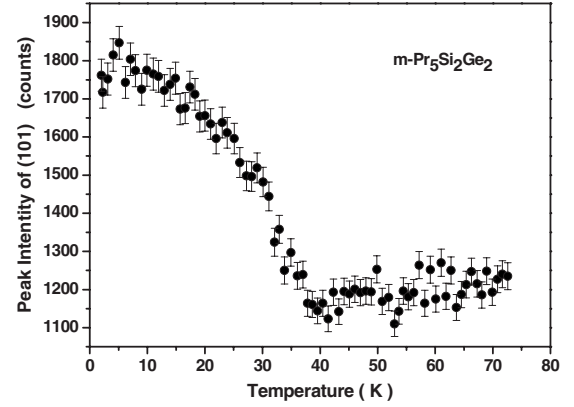


FIG. 5. Temperature dependence of the peak intensity of (101) reflection of  $m$ - $\text{Pr}_5\text{Si}_2\text{Ge}_2$  on warming, measured by high-flux BT-7 spectrometer at NIST-NCNR.

magnetic space group for the compound can be greatly reduced.

There are eight Shubnikov groups derived from  $P4_12_12$ , i.e.,  $P4_12_12$ ,  $P4_12_12'$ ,  $P4_1'2_12'$ ,  $P4_12_1'2'$ ,  $P4_1'2_1'2'$ ,  $P_c4_12_12$ ,  $P_c4_1'2_12'$ , and  $P'A_12_12$ . The  $P4_12_12'$  is nonmagnetic, i.e., a “gray” group. Among the seven magnetic Shubnikov groups, only the  $P4_12_1'2'$  is ferromagnetic. Therefore, we used the magnetic space group  $P4_12_1'2'$  to model the magnetic structure of  $t$ - $\text{Pr}_5\text{Si}_2\text{Ge}_2$  below  $T_C$ . The same magnetic space group was used for the magnetic structure of  $\text{Nd}_5\text{Si}_4$  by Cadogan *et al.*<sup>8</sup> For this magnetic structure model, the spin components  $\mu_x$  and  $\mu_y$  of the Pr atoms on both the 4a and 8b sites arrange antiferromagnetically along the respective crystal axis, leading to zero net magnetization along the  $a$  and  $b$  directions, whereas the spin component  $\mu_z$  of the Pr atoms arrange ferromagnetically along the  $c$  axis.

The experimental and calculated NPD patterns of the  $t$ - $\text{Pr}_5\text{Si}_2\text{Ge}_2$  at 4 K is shown in Fig. 2(b). The magnetic structure is depicted in Fig. 3(a), showing the magnetic atoms only. The refinement results of the NPD data at some selected temperatures (4, 40, 60, and 300 K) are listed in Table I and the magnetic moments of the atoms in Table II. The temperature dependence of lattice parameters is shown in Fig. 4. As the temperature decreases, the lattice parameter  $a$  and unit cell volume  $V$  decrease, while the lattice parameter  $c$  increases. At  $T_C=52$  K,  $c$  decreases gradually but significantly, and  $a$  increases with the further decrease of temperature, indicating a second-order transition. However, a small negative magnetovolume effect is observed, i.e., a decrease of unit cell volume when cooling through the magnetic transition temperature  $T_C$ .

## B. Crystal and magnetic structures of $m$ - $\text{Pr}_5\text{Si}_2\text{Ge}_2$

NPD experiment at room temperature confirmed that the as-arc-melted sample crystallized in the monoclinic  $\text{Gd}_5\text{Si}_2\text{Ge}_2$ -type structure with space group  $P112_1/a$ . Difference curve of the NPD patterns below and above 40 K signifies the contribution of magnetic scattering at low temperature. The magnetic Bragg peaks can be indexed by the nuclear unit cell. Figure 5 shows the temperature dependence

TABLE III. Data of crystallographic structure at different temperatures for  $m$ -Pr<sub>5</sub>Si<sub>2</sub>Ge<sub>2</sub> derived from the fitting to NPD patterns. Space group:  $P112_1/a$ .  $M=0.5\text{Si}+0.5\text{Ge}$ ,  $B$  is the isotropic temperature factor, and  $R_P$  and  $R_{WP}$  are residuals of fitting to the pattern and the weighted pattern, respectively.  $R_B$  and  $R_M$  are Bragg and magnetic  $R$  factors, respectively.  $\chi^2$  is a “goodness of fit” indicator (Ref. 20).

	4 K	30 K	50 K	300 K
$a$ (Å)	7.8105(4)	7.8138(4)	7.8178(4)	7.8232(8)
$b$ (Å)	15.1634(6)	15.1611(7)	15.1596(8)	15.1977(15)
$c$ (Å)	7.9787(4)	7.9778(4)	7.9795(5)	7.9918(7)
$\gamma$ (deg)	93.867(3)	93.887(3)	93.913(4)	93.798(6)
$V$ (Å <sup>3</sup> )	942.80(7)	942.91(8)	943.48(9)	948.09(16)
Pr1 (4e) $x$	0.328(1)	0.327(1)	0.326(1)	0.326(2)
$y$	0.2457(5)	0.2452(5)	0.2445(6)	0.2468(9)
$z$	0.0038(8)	0.0039(9)	0.0064(11)	0.0051(13)
$B$ (Å <sup>2</sup> )	0.00	0.03	0.05	0.28(9)
Pr2a (4e) $x$	-0.0069(9)	-0.0087(11)	-0.0068(12)	-0.0023(18)
$y$	0.1002(4)	0.1007(4)	0.0994(6)	0.1013(9)
$z$	0.1799(9)	0.1816(10)	0.1830(12)	0.1831(17)
$B$ (Å <sup>2</sup> )	0.02	0.12	0.20	1.19(11)
Pr2b (4e) $x$	0.025(1)	0.024(1)	0.021(1)	0.024(2)
$y$	0.4016(5)	0.3999(6)	0.3986(7)	0.3990(9)
$z$	0.197(1)	0.193(1)	0.192(1)	0.186(2)
$B$ (Å <sup>2</sup> )	0.01	0.10	0.16	0.99(11)
Pr3a (4e) $x$	0.358(1)	0.363(1)	0.362(1)	0.359(2)
$y$	0.8831(4)	0.8837(5)	0.8817(5)	0.8828(8)
$z$	0.1625(10)	0.1622(10)	0.1619(12)	0.1620(16)
$B$ (Å <sup>2</sup> )	0.01	0.08	0.13	0.80(11)
Pr3b (4e) $x$	0.327(1)	0.327(1)	0.327(1)	0.328(2)
$y$	0.6217(4)	0.6222(5)	0.6217(6)	0.6228(8)
$z$	0.1731(9)	0.1702(10)	0.1698(11)	0.1761(16)
$B$ (Å <sup>2</sup> )	0.01	0.07	0.12	0.74(10)
M1 (4e) $x$	0.2161(9)	0.2176(9)	0.2169(9)	0.213(1)
$y$	0.2501(5)	0.2511(5)	0.2510(5)	0.2523(6)
$z$	0.3695(8)	0.3679(8)	0.3688(8)	0.3712(12)
$B$ (Å <sup>2</sup> )	0.01	0.09	0.15	0.90(9)
M2 (4e) $x$	0.9520(8)	0.9544(8)	0.9532(8)	0.951(1)
$y$	0.2506(4)	0.2524(4)	0.2527(4)	0.2517(6)
$z$	0.8992(8)	0.8978(8)	0.8964(8)	0.8960(11)
$B$ (Å <sup>2</sup> )	0.01	0.07	0.11	0.66(9)
M3a (4e) $x$	0.2163(9)	0.2166(9)	0.2158(9)	0.2134(13)
$y$	0.9560(5)	0.9566(5)	0.9561(4)	0.9560(7)
$z$	0.4680(9)	0.4669(9)	0.4669(8)	0.4625(12)
$B$ (Å <sup>2</sup> )	0.01	0.07	0.12	0.71(10)
M3b (4e) $x$	0.1450(8)	0.1455(9)	0.1477(9)	0.1471(13)

TABLE III. (*Continued.*)

	4 K	30 K	50 K	300 K
$y$	0.5429(4)	0.5440(4)	0.5434(4)	0.5408(6)
$z$	0.4689(9)	0.4693(8)	0.4702(8)	0.4736(12)
$B$ ( $\text{\AA}^2$ )	0.01	0.08	0.14	0.81(8)
$R_p(\%)/R_{wp}(\%)$	4.40/5.40	4.24/5.13	4.13/5.04	4.84/5.87
$R_B(\%)/R_M(\%)$	5.60/7.33	6.88/10.1	8.56/ $N$	5.84/ $N$
$\chi^2$	1.94	1.75	1.64	0.822

of the peak intensity of the (101) reflection on warming, which manifests a magnetic ordering temperature of  $T_C = 40$  K, in good agreement with the magnetization measurement ( $T_C = 38$  K).<sup>19</sup> No other magnetic transition occurs below  $T_C$ . Magnetization measurement indicated a second-order magnetic transition at  $T_C$ .<sup>19</sup>

High-resolution NPD data were recorded at four temperatures: 4, 30, 50, and 300 K. The NPD data above  $T_C$  can be well fitted by the monoclinic  $\text{Gd}_5\text{Si}_2\text{Ge}_2$ -type structure with the space group  $P112_1/a$  as shown in Fig. 6(a). The refinement results are listed in Table III. Similar to the discussion on the magnetic structure model of the  $t\text{-Pr}_5\text{Si}_2\text{Ge}_2$ , the space group  $P112_1'/a'$  is the only ferromagnetic space group among the ten Shubnikov groups derived from  $P112_1/a$  that is compatible with the appreciable magnetization at 5 K and with the nuclear unit cell of the magnetic structure of  $m\text{-Pr}_5\text{Si}_2\text{Ge}_2$ . The same magnetic space group was adopted for monoclinic  $\text{Nd}_5\text{Si}_{1.45}\text{Ge}_{2.55}$  and  $\text{Pr}_5\text{Si}_{1.5}\text{Ge}_{2.5}$  by Magen *et al.* based on the representation analysis and the trial-and-error fittings to the NPD data.<sup>12</sup> By the magnetic space group  $P112_1'/a'$ , all Pr atoms occupy general positions 4e with the spin components arranged ferromagnetically along the  $a$  and  $b$  axes but antiferromagnetically along the  $c$  axis. This mag-

netic structure model gives a satisfactory fitting to the NPD data below  $T_C$  as shown in Fig. 6(b).

Primary refinements of the crystal and magnetic structures of  $m\text{-Pr}_5\text{Si}_2\text{Ge}_2$  were carried out with 70 fitted parameters, about twice of the fitted parameters for the  $t\text{-Pr}_5\text{Si}_2\text{Ge}_2$  (43). Though the refinements converged satisfactorily and the derived crystallographic and magnetic data were close to those of the reported  $\text{Nd}_5\text{Si}_{1.45}\text{Ge}_{2.55}$  and  $\text{Pr}_5\text{Si}_{1.5}\text{Ge}_{2.5}$ ,<sup>12</sup> the fitted thermal parameters  $B$  on some sites did not follow the general decreasing trend with the decrease of temperature due to possible correlation among the fitted parameters. Therefore, we fixed the thermal parameters on each site as  $B_i(T) = B_i(300 \text{ K})T/300$  during the refinements, where  $B_i(300)$  is the thermal parameter on site  $i$  at 300 K and is derived from the refinement to the NPD data at 300 K (crystallographic structure only with 35 fitted parameters).

The magnetic structure of the  $m\text{-Pr}_5\text{Si}_2\text{Ge}_2$  is depicted in Fig. 3(b), showing the magnetic atoms only. The refinement results of the NPD data are listed in Table III and the magnetic moments of the atoms in Table IV. The temperature dependence of lattice parameters is shown in Fig. 7. Though there is not enough data around  $T_C$ , a small negative magneto-volume effect is discernable.

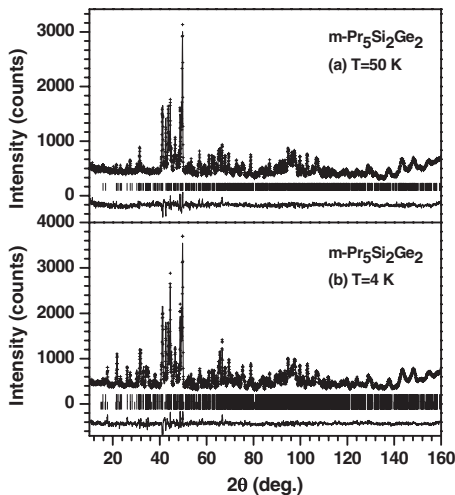


FIG. 6. Experimental (crosses) and calculated (solid line) intensities of  $m\text{-Pr}_5\text{Si}_2\text{Ge}_2$  at (a) 50 K and (b) 4 K. Differences between the experimental and calculated patterns are shown at the bottom of the figure. The vertical bars indicate the expected nuclear reflection positions. The expected magnetic reflection positions are marked by the bars on the lower row in (b).

TABLE IV. Magnetic moment components of Pr atoms in  $m\text{-Pr}_5\text{Si}_2\text{Ge}_2$  at selected temperatures derived from the fitting to NPD data. The atomic positions refer to Table III. Magnetic space group:  $P112_1'/a'$ .

	$\mu_x$ ( $\mu_B$ )	$\mu_y$ ( $\mu_B$ )	$\mu_z$ ( $\mu_B$ )	$\mu$ ( $\mu_B$ )
$T = 4 \text{ K}$				
Pr1	2.24(5)	0.05(9)	-0.29(8)	2.26(5)
Pr2a	3.03(8)	-0.29(9)	0.27(8)	3.07(9)
Pr2b	1.28(7)	1.94(9)	-0.19(8)	2.26(9)
Pr3a	1.92(6)	0.76(9)	0.34(9)	2.04(6)
Pr3b	2.50(7)	-0.52(9)	1.38(9)	2.93(7)
$T = 30 \text{ K}$				
Pr1	1.80(7)	-0.04(15)	-0.25(11)	1.82(7)
Pr2a	2.25(10)	-0.27(14)	-0.04(11)	2.28(11)
Pr2b	0.86(9)	1.12(16)	-0.04(10)	1.36(15)
Pr3a	1.24(7)	0.46(15)	0.52(13)	1.39(9)
Pr3b	1.71(9)	0.07(16)	0.84(15)	1.90(10)

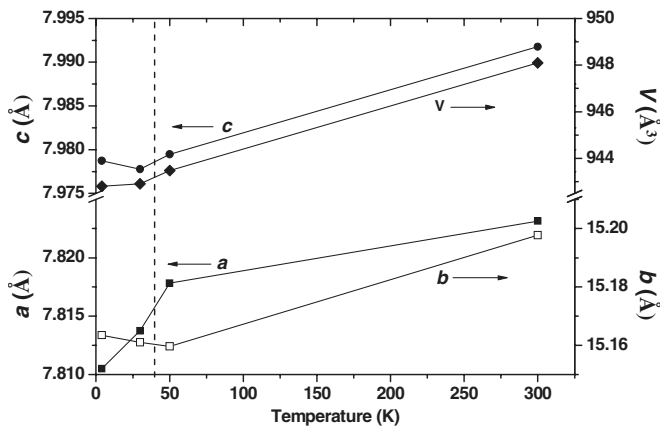


FIG. 7. Temperature dependence of the lattice parameters of  $m\text{-Pr}_5\text{Si}_2\text{Ge}_2$ . The vertical dashed line indicates the position of  $T_C$ .

#### IV. DISCUSSION

The crystal structures of  $m\text{-Pr}_5\text{Si}_2\text{Ge}_2$  and  $t\text{-Pr}_5\text{Si}_2\text{Ge}_2$  are depicted in Figs. 8(a) and 9(a), respectively. They have many similarities: (i) all Pr atoms have six  $M$  atoms ( $=0.5\text{Si} + 0.5\text{Ge}$ ) as the nearest neighbors with a bond distance of  $d_{\text{Pr}-M} \sim 3.1$  Å; (ii) Pr atoms have 8–10 neighboring Pr atoms within the  $d_{\text{Pr}-\text{Pr}}$  range  $< 4.35$  Å; (iii) Pr1 at 4e sites in  $m\text{-Pr}_5\text{Si}_2\text{Ge}_2$  and at 4a sites in  $t\text{-Pr}_5\text{Si}_2\text{Ge}_2$  have eight neighboring Pr atoms, with  $d_{\text{Pr}-\text{Pr}} \sim 3.6$  Å. The eight Pr atoms form a slightly distorted cube and the six  $M$  atoms form a slightly distorted octahedron, which acts as the building unit  $[\text{Pr}M_6]\text{Pr}_8$  of both the structures as we describe below, and (iv) other Pr atoms but Pr1 in both the structures have 2–3 neighboring Pr atoms with much shorter  $d_{\text{Pr}-\text{Pr}}$  ( $\sim 3.6$  Å) than the distances to the additional 6–8 neighboring Pr atoms ( $\sim 3.9$  Å).

The difference between the two structures is also salient, however. In the  $t\text{-Pr}_5\text{Si}_2\text{Ge}_2$ , all  $M$  atoms are covalently

bonded with  $d_{M-M} \sim 2.6$  Å, while only 3/4 of the  $M$  atoms in the  $m\text{-Pr}_5\text{Si}_2\text{Ge}_2$  form covalent bonds ( $M1-M2$  and  $M3b-M3b$  bonds,  $d_{M-M} \sim 2.6$  Å). The most striking difference between the two structures is the way the building unit  $[\text{Pr}M_6]\text{Pr}_8$  connect with each other. In  $m\text{-Pr}_5\text{Si}_2\text{Ge}_2$ , the building units share four nonadjacent and *parallel* edges of a  $\text{Pr}_8$  cube, forming an infinite two-dimensional  ${}^2_\infty[\text{Pr}_5M_4]$  slab parallel to the  $ac$  plane [Figs. 8(a) and 8(b)]. Half of the adjacent slabs are connected by covalent  $M-M$  bonds ( $M3b-M3b$  bonds). In  $t\text{-Pr}_5\text{Si}_2\text{Ge}_2$ , the building units also share four nonadjacent but *perpendicular* edges of a  $\text{Pr}_8$  cube, forming a cackle-stair-like stacking of the cubes [Figs. 9(a) and 9(b)]. In addition, each  $M1-M2$  bond connects to three  $\text{Pr}_8$  cubes in  $t\text{-Pr}_5\text{Si}_2\text{Ge}_2$ , while in  $m\text{-Pr}_5\text{Si}_2\text{Ge}_2$ , each  $M1-M2$  bond connects to four  $\text{Pr}_8$  cubes and each  $M3b-M3b$  bond to two  $\text{Pr}_8$  cubes. These similarities and differences between the structures of  $m$ - and  $t\text{-Pr}_5\text{Si}_2\text{Ge}_2$  should be responsible for their relatively stable existence at room temperature, i.e., the difference in free energy between these two structures is very small, and for the structure-dependent physical properties.

Below  $T_C$ , both the compounds exhibit noncollinear magnetic structures. For  $m\text{-Pr}_5\text{Si}_2\text{Ge}_2$ , the net magnetic components exist along the  $a$  and  $b$  directions. The ferromagnetic components occur mainly along the  $a$  direction for the Pr atoms except for Pr2b [Fig. 3(b)]. For Pr2b, the magnetic components along  $a$  and  $b$  directions are comparable. At 4 K, the magnetic moments of Pr2a and Pr3b are close to the saturation moment of a free  $\text{Pr}^{3+}$  ion ( $3.5\mu_B$ ), while the moments of other Pr atoms are a little smaller because of the CEF effects that partially quench the orbital angular moment. The average moment of Pr atom at 4 K is  $2.51\mu_B$ . The average net moment on the  $ab$  plane is  $2.21\mu_B$  per Pr atom, in reasonable agreement with the magnetization at 5 K and 50 kOe ( $1.72\mu_B$  per Pr atom),<sup>19</sup> since the magnetization curve ( $M-H$ ) records exclusively the projection of ferromagnetic component in magnetic domains along the applied field

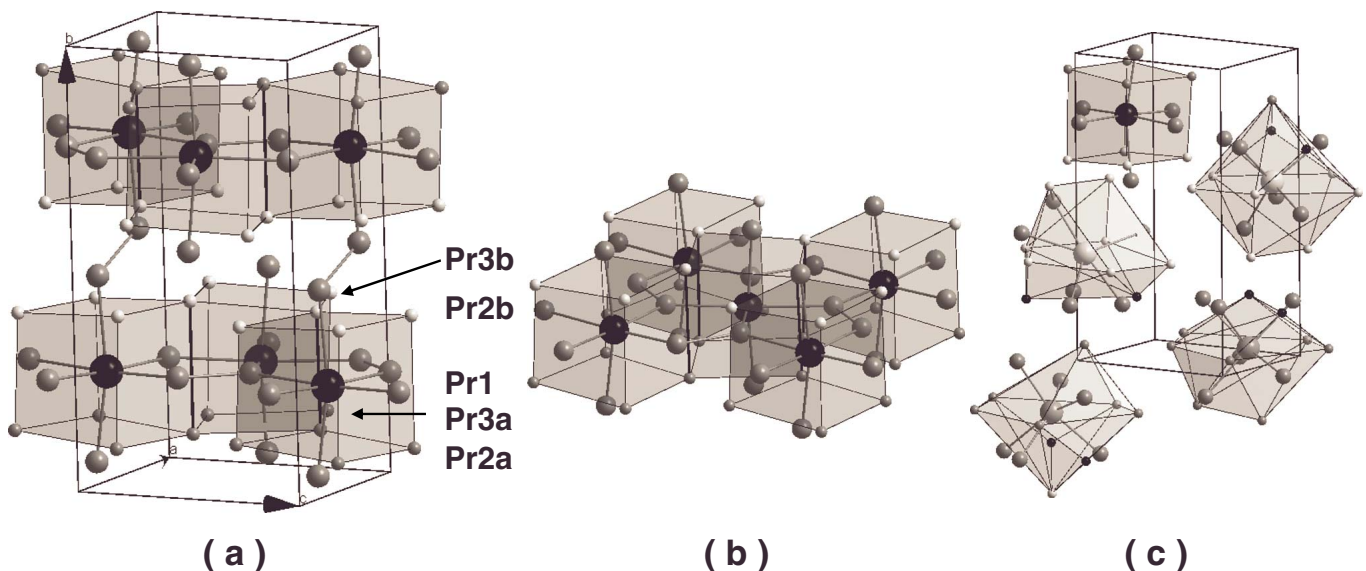


FIG. 8. (Color online) (a) Crystal structure of  $m\text{-Pr}_5\text{Si}_2\text{Ge}_2$ , (b) the connection of five building units  $[\text{Pr}M_6]\text{Pr}_8$ , and (c) the Pr-coordination polyhedrons of Pr atoms. The size of the coordinating Pr atoms on the vertices of the polyhedrons is reduced by 60%.

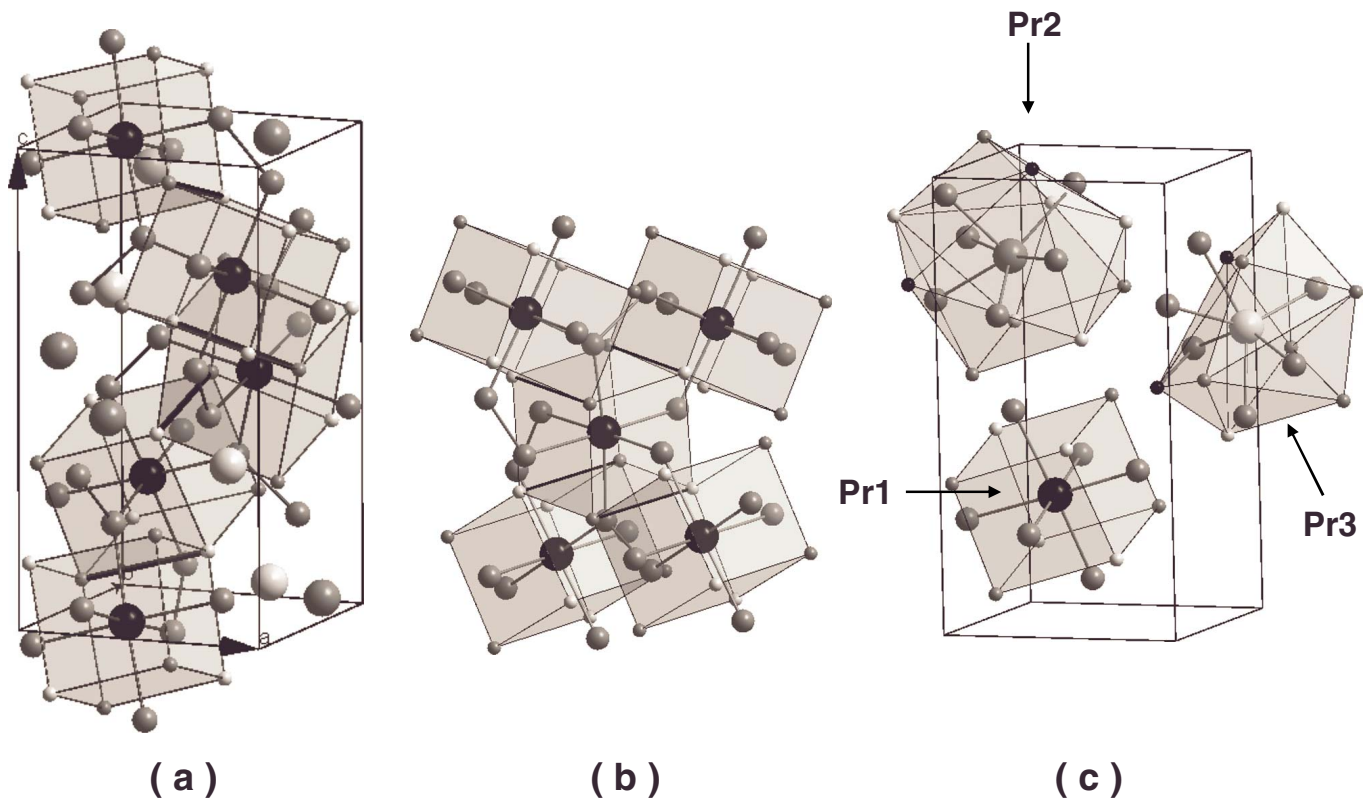


FIG. 9. (Color online) (a) Crystal structure of  $t$ - $\text{Pr}_5\text{Si}_2\text{Ge}_2$ , (b) the connection of five building units  $[\text{PrM}_6]\text{Pr}_8$ , and (c) the Pr-coordination polyhedrons of Pr atoms. The size of the coordinating Pr atoms on the vertices of the polyhedrons is reduced by 60%.

direction for a stable noncollinear magnetic structure.

For  $t$ - $\text{Pr}_5\text{Si}_2\text{Ge}_2$ , net magnetic moment occurs exclusively along the  $c$  direction. Figure 10 shows the temperature dependence of magnetic moment components of Pr atoms on each site. The magnetic ordering of Pr atoms develops simultaneously on different sites, in contrast to  $\text{Pr}_5\text{Ge}_4$ , in which magnetic ordering of Pr atoms on different sites took place at different temperatures.<sup>9</sup> From Fig. 10, it can be seen that the moments of Pr1 and Pr3 align almost along the  $c$  axis, whereas the moment of Pr2 lies almost on the  $bc$  plane with comparable  $b$  and  $c$  components. At 4 K, the average moment of Pr is  $2.69\mu_B$ , a little smaller than the saturation moment of a free  $\text{Pr}^{3+}$  ion ( $3.5\mu_B$ ), possible due to the presence of the CEF effects. The average net moment along the  $c$  axis is  $2.35\mu_B$  per Pr atom, which is appreciably larger than the magnetization at 5 K and 50 kOe ( $1.33\mu_B$  per Pr atom).<sup>19</sup> The smaller observed magnetization can be attributed to an unsaturation state of the compound in the experiments. The field dependence of magnetization showed that it was more difficult for the  $t$ - $\text{Pr}_5\text{Si}_2\text{Ge}_2$  to approach the saturation than the  $m$ - $\text{Pr}_5\text{Si}_2\text{Ge}_2$ , which could probably be associated with a larger magnetocrystalline anisotropy or with the domain-wall pinning effects due to the defects formed during quenching to water from high temperature.

It is well known that in metallic rare earth and rare-earth-rich intermetallic compounds, the Ruderman-Kittel-Kasuya-Yosida (RKKY) interaction between  $R$  atoms plays an important role. The RKKY interaction is a long-range indirect exchange interaction and is sensitive to the distance between

the  $R$  atoms and their chemical environments. The RKKY interaction model is likely applicable to the  $R_5(\text{Si}_x\text{Ge}_{1-x})_4$  compounds.<sup>4</sup> The Pr-coordination polyhedrons of Pr atoms in the structures of  $m$ - and  $t$ - $\text{Pr}_5\text{Si}_2\text{Ge}_2$  are shown in Figs. 8(c) and 9(c), respectively. The chemical environments around Pr atoms on different sites are remarkably different. The Pr-Pr distance varies in the range of 3.5–4.2 Å. Therefore, both AFM and FM exchange interactions between Pr atoms could exist in the compound. The competition between the AFM

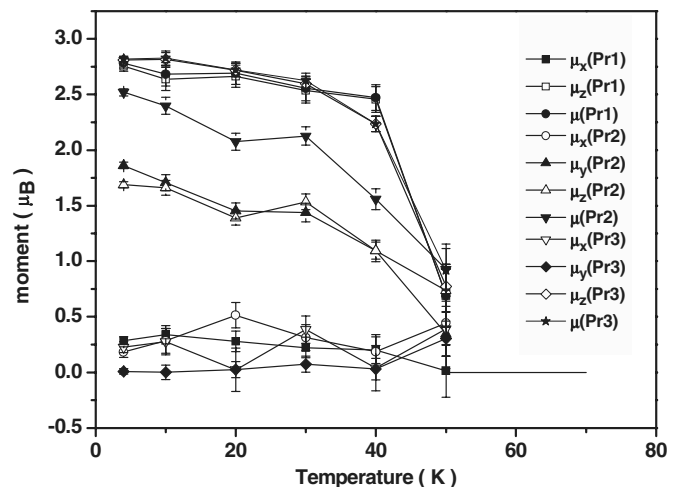


FIG. 10. Temperature dependence of magnetic moments of Pr atoms in  $t$ - $\text{Pr}_5\text{Si}_2\text{Ge}_2$ .

and FM interactions and different magnetocrystalline anisotropies on different sites should be the reason for the occurrence of the complex noncollinear magnetic structures.

Our refinement results of the magnetic structures of *t*- and *m*-Pr<sub>5</sub>Si<sub>2</sub>Ge<sub>2</sub> are basically similar to those of Nd<sub>5</sub>Si<sub>4</sub>,<sup>8</sup> Pr<sub>5</sub>Si<sub>1.5</sub>Ge<sub>2.5</sub>, and Nd<sub>5</sub>Si<sub>1.45</sub>Ge<sub>2.55</sub>,<sup>12</sup> especially regarding the easy magnetization direction (EMD). For rare earth intermetallic compounds, the EMD is essentially determined by the chemical environment around the *R* atoms and the shape of the 4*f*-electron distribution characterized by the second-order Stevens coefficient  $\alpha_J$ . In orthorhombic and monoclinic R<sub>5</sub>(Si<sub>1-x</sub>Ge<sub>x</sub>)<sub>4</sub> (*x* ~ 0.5), the chemical environments around *R* atoms are similar, and the available magnetic structural data show that the EMD of the monoclinic phase is along the *a* axis for  $\alpha_J < 0$  [*R*=Tb,<sup>10,11</sup> Pr, Nd (Ref. 12)] and along the *b* axis for  $\alpha_J > 0$  [*R*=Er (Ref. 15)]. In addition, while the dramatic magnetovolume effect in R<sub>5</sub>(Si<sub>1-x</sub>Ge<sub>x</sub>)<sub>4</sub> for *R*=Gd and Tb can be attributed to the simultaneous occurrence of the first-order magnetic and martensiticlike structural phase transitions,<sup>3,5,11</sup> small negative magnetovolume effect is observed in *m*- and *t*-Pr<sub>5</sub>Si<sub>2</sub>Ge<sub>2</sub> around *T*<sub>C</sub> as shown in Figs. 4 and 7, in contrast to the small positive magnetovolume effect in Er<sub>5</sub>(Si<sub>1-x</sub>Ge<sub>x</sub>)<sub>4</sub>. For these three latter compounds, no structural phase transition takes place around *T*<sub>C</sub>. In general, the magnetovolume effect can result from a competition between magnetic energy and elastic energy. A negative magnetovolume effect might indicate an increased resultant exchange interaction as the distance between magnetic atoms decreases. Figures 4 and 7 show that the largest change of the lattice constant occurs always along the EMD for *t*- and *m*-Pr<sub>5</sub>Si<sub>2</sub>Ge<sub>2</sub> compounds.

## V. SUMMARY

The tetragonal *t*-Pr<sub>5</sub>Si<sub>2</sub>Ge<sub>2</sub> crystallizes in the Zr<sub>5</sub>Si<sub>4</sub>-type structure with the space group *P*4<sub>1</sub>2<sub>1</sub>2 down to 4 K. Long-range magnetic ordering takes place at *T*<sub>C</sub>=52 K, and the magnetic structure can be modeled with the magnetic space group *P*4<sub>1</sub>2<sub>1</sub>'2'. The magnetic structure shows a net ferro-

magnetic component exclusively along the *c* axis. No other magnetic transition is manifested below *T*<sub>C</sub>. The lattice parameter *a* and unit cell volume *V* decrease with the decrease of temperature, while the lattice parameter *c* increases. Below *T*<sub>C</sub>=52 K, *c* decreases significantly and *a* increases gradually with the further decrease of temperature, indicating a second-order magnetic transition. Refinements of the temperature-dependent NPD data reveal that the magnetic ordering of the Pr atoms develops simultaneously on different sites.

The monoclinic *m*-Pr<sub>5</sub>Si<sub>2</sub>Ge<sub>2</sub> crystallizes in the Gd<sub>5</sub>Si<sub>2</sub>Ge<sub>2</sub>-type structure with the space group *P*112<sub>1</sub>/*a* down to 4 K. Long-range magnetic ordering occurs at *T*<sub>C</sub>=40 K, and the magnetic structure can be modeled with the magnetic space group *P*112<sub>1</sub>'/*a*', exhibiting net ferromagnetic components along the *a* and *b* directions. No other magnetic transition is observed below *T*<sub>C</sub>.

For both the compounds, a small negative magnetovolume effect, i.e., a decrease of unit cell volume when cooling through the magnetic transition temperature *T*<sub>C</sub>, is observed. The largest change of the lattice constant occurs always along the EMD of compounds. In the scenario of the RKKY interaction model, the competition between the AFM and FM interactions coexisting in the compounds and the different magnetocrystalline anisotropies on different Pr sites should be the reason for the occurrence of the complex noncollinear magnetic structures of the *t*- and *m*-Pr<sub>5</sub>Si<sub>2</sub>Ge<sub>2</sub>.

The crystallographic structures of *m*-Pr<sub>5</sub>Si<sub>2</sub>Ge<sub>2</sub> and *t*-Pr<sub>5</sub>Si<sub>2</sub>Ge<sub>2</sub> have similarities and differences in many aspects, which should be responsible for their relatively stable existence at room temperature and the structure-dependent physical properties of the polymorphic Pr<sub>5</sub>Si<sub>2</sub>Ge<sub>2</sub>.

## ACKNOWLEDGMENTS

The work was supported by the National Natural Science Foundation of China under Grants No. 50025102 and No. 50631040, the State Key Project of Fundamental Research under Grant No. 2006CB601101, and the exchange program between NIST and the Chinese Academy of Sciences.

\*ghrao@aphy.iphy.ac.cn

<sup>1</sup>V. K. Pecharsky and K. A. Gschneidner, Jr., Phys. Rev. Lett. **78**, 4494 (1997).

<sup>2</sup>G. S. Smith, A. G. Tharp, and Q. Johnson, Acta Crystallogr. **22**, 840 (1967).

<sup>3</sup>L. Morellon, P. A. Algarabel, M. R. Ibarra, J. Blasco, B. Garcia-Landa, Z. Arnold, and F. Albertini, Phys. Rev. B **58**, R14721 (1998).

<sup>4</sup>W. Choe, V. K. Pecharsky, A. O. Pecharsky, K. A. Gschneidner, Jr., V. G. Young, Jr., and G. J. Miller, Phys. Rev. Lett. **84**, 4617 (2000).

<sup>5</sup>L. Morellon, J. Blasco, P. A. Algarabel, and M. R. Ibarra, Phys. Rev. B **62**, 1022 (2000).

<sup>6</sup>E. M. Levin, V. K. Pecharsky, and K. A. Gschneidner, Jr., Phys. Rev. B **60**, 7993 (1999).

<sup>7</sup>L. Tan, A. Kreyssig, J. W. Kim, A. I. Goldman, R. J. McQueeney, D. Wermeille, B. Sieve, T. A. Lograsso, D. L. Schlagel, S. L. Budko, V. K. Pecharsky, and K. A. Gschneidner, Jr., Phys. Rev. B **71**, 214408 (2005).

<sup>8</sup>J. M. Cadogan, D. H. Ryan, Z. Altounian, H. B. Wang, and I. P. Swainson, J. Phys.: Condens. Matter **14**, 7191 (2002).

<sup>9</sup>G. H. Rao, Q. Huang, H. F. Yang, D. L. Ho, J. W. Lynn, and J. K. Liang, Phys. Rev. B **69**, 094430 (2004).

<sup>10</sup>C. Ritter, L. Morellon, P. A. Algarabel, C. Magen, and M. R. Ibarra, Phys. Rev. B **65**, 094405 (2002).

<sup>11</sup>L. Morellon, C. Ritter, C. Magen, P. A. Algarabel, and M. R. Ibarra, Phys. Rev. B **68**, 024417 (2003).

<sup>12</sup>C. Magen, C. Ritter, L. Morellon, P. A. Algarabel, and M. R. Ibarra, J. Phys.: Condens. Matter **16**, 7427 (2004).

<sup>13</sup>J. M. Cadogan, D. H. Ryan, Z. Altounian, X. Liu, and I. P. Swain-

- son, *J. Appl. Phys.* **95**, 7076 (2004).
- <sup>14</sup>V. O. Garlea, J. L. Zarestky, C. Y. Jones, L. L. Lin, D. L. Schlage, T. A. Lograsso, A. O. Tsokol, V. K. Pecharsky, K. A. Gschneidner, Jr., and C. Stassis, *Phys. Rev. B* **72**, 104431 (2005).
- <sup>15</sup>C. Ritter, C. Magen, L. Morellon, P. A. Algarabel, M. R. Ibarra, V. K. Pecharsky, A. O. Tsokol, and K. A. Gschneidner, Jr., *J. Phys.: Condens. Matter* **18**, 3937 (2006).
- <sup>16</sup>V. K. Pecharsky, A. O. Pecharsky, Y. Mozharivskyj, K. A. Gschneidner, Jr., and G. J. Miller, *Phys. Rev. Lett.* **91**, 207205 (2003).
- <sup>17</sup>Y. Mozharivskyj, A. O. Pecharsky, V. K. Pecharsky, and G. J. Miller, *J. Am. Chem. Soc.* **127**, 317 (2005).
- <sup>18</sup>V. K. Pecharsky, A. O. Pecharsky, and K. A. Gschneidner, Jr., *J. Alloys Compd.* **344**, 362 (2002).
- <sup>19</sup>H. F. Yang, G. H. Rao, G. Y. Liu, Z. W. Ouyang, X. M. Feng, W. F. Liu, W. G. Chu, and J. K. Liang, *J. Phys.: Condens. Matter* **14**, 9705 (2002).
- <sup>20</sup>J. L. Rodríguez-Carvajal, *Physica B* **192**, 55 (1993).
- <sup>21</sup>H. F. Yang, G. H. Rao, W. G. Chu, G. Y. Liu, Z. W. Ouyang, and J. K. Liang, *J. Alloys Compd.* **339**, 189 (2002).
- <sup>22</sup>W. Opechowski and R. Guccione, in *Magnetism*, edited by G. T. Rado and H. Suhl (Academic, New York, 1963), Vol. IIA, p. 105.